On the formulation of snow thermal conductivity in large-scale sea ice models

O. Lecomte,[1] T. Fichefet,[1] M. Vancoppenolle,[2] F. Domine,[3,4] F. Massonnet,[1] P. Mathiot,[5] S. Morin,[6] and P.Y. Barriat[1]

[1] An assessment of the performance of a state-of-the-art large-scale coupled sea ice-ocean model, including a new snow multilayer thermodynamic scheme, is performed. Four 29 year long simulations are compared against each other and against sea ice thickness and extent observations. Each simulation uses a separate parameterization for snow thermophysical properties. The first simulation uses a constant thermal conductivity and prescribed density profiles. The second and third parameterizations use typical power-law relationships linking thermal conductivity directly to density (prescribed as in the first simulation). The fourth parameterization is newly developed and consists of a set of two linear equations relating the snow thermal conductivity and density to the mean seasonal wind speed. Results show that simulation 1 leads to a significant overestimation of the sea ice thickness due to overestimated thermal conductivity, particularly in the Northern Hemisphere. Parameterizations 2 and 4 lead to a realistic simulation of the Arctic sea ice mean state. Simulation 3 results in the underestimation of the sea ice basal growth in both hemispheres, but is partly compensated by lateral growth and snow ice formation in the Southern Hemisphere. Finally, parameterization 4 improves the simulated Snow Depth Distributions by including snow packing by wind, and shows potential for being used in future works. The intercomparison of all simulations suggests that the sea ice model is more sensitive to the snow representation in the Arctic than it is in the Southern Ocean, where the sea ice thickness is not driven by temperature profiles in the snow.

1. Introduction

[2] The thermophysical properties of snow on sea ice play a key role in the physics of heat conduction through the snow-sea ice system. In particular, several studies have shown the importance of the snow thermal insulating effect on the sea ice growth and decay [e.g., *Eicken et al.*, 1995; *Fichefet and Morales Maqueda*, 1997; *Sturm et al.*, 2002]. By strongly curtailing the conductive heat flux from the sea ice to the snow-atmosphere interface and therefore heat losses to the atmosphere, the low thermal conductivity of snow reduces the basal ice growth.

[3] The process of heat transfer through the snow includes mainly three mechanisms: (1) heat conduction through the ice matrix formed by the interconnected grains, (2) heat conduction in the interstitial air, and (3) the transfer of latent heat by water vapor that sublimates from warmer grains to condense on colder ones. With regard to this, a variable called effective thermal conductivity (k_{eff}) is typically used, accounting for all three processes. However, the term effective thermal conductivity is probably not the most appropriate, because it includes transfer by latent heat, which is not a conductive process. Following *Calonne et al.* [2011], we therefore refer to the variable regrouping the above three processes as the apparent thermal conductivity, k_{app}. Another potentially important process, heat advection by wind pumping of air over a rough snow surface, is not included in k_{app} and has to be simulated separately if represented in a model. The range of possible values for k_{app} extends from about 0.03 to

[1]Georges Lemaître Centre for Earth and Climate Research, Earth and Life Institute, Université Catholique de Louvain, Louvain-la-Neuve, Belgium.

[2]Laboratoire d'Océanographie et du Climat (Expérimentations et Approches Numériques), Paris, France.

[3]Takuvik Joint International Laboratory, Université Laval (Canada) and Centre National de la Recherche Scientifique (France), Quebec, Quebec, Canada.

[4]Department of Chemistry, Université Laval, Quebec, Quebec, Canada.

[5]British Antarctic Survey, Natural Environment Research Council, Cambridge, UK.

[6]Snow Research Center, CNRM-GAME, Météo-France/CNRS, St Martin d'Hères, France.

0.65 W m^{-1} K^{-1} [*Sturm et al.*, 1997, 1998], and several regression curves relating snow thermal conductivity to snow density ρ_s were proposed (e.g., *Yen* [1981] and *Sturm et al.* [1997], among the most commonly known and used in the modeling community). Yet most large-scale sea ice models (coupled to ocean and/or atmospheric general circulation models or not) have been using the 0.31 W m^{-1} K^{-1} constant value proposed by *Maykut and Untersteiner* [1971] and *Semtner* [1976]. Until now, the same constant has been used in the Louvain-la-Neuve Sea Ice model (LIM), which includes, like all those models, a relatively simple snow representation with only one snow layer and constant snow density and thermal conductivity. Even so, *Wu et al.* [1999] and *Fichefet et al.* [2000] showed that their simulated Antarctic sea ice exhibits a strong sensitivity to snow thermal conductivity, despite the rather simplistic snow representation in their models. In particular, they found the modeled average Antarctic sea ice to be on average 10% thinner when using a value reduced by half for k_{app} with respect to the usual value.

[4] The present study aims at extending those works and investigates the sensitivity of a large-scale coupled sea ice-ocean model to the representation of snow thermal conductivity using a new, more elaborate snow thermodynamic scheme. In particular, we show the impacts of a newly developed and simple parameterization of snow packing by wind on the simulated snow depth distributions. The second objective is to study the reproducibility of *Lecomte et al.*'s [2011] results and assess the differences in response of the sea ice model to various thermal conductivity formulations between both hemispheres. Benefit is taken from the host coupled model including oceanic feedbacks to explain those dissimilarities. Lastly, we evaluate the ability of this model to simulate the sea ice extent and thickness in both hemispheres with respect to observations. The paper is laid out as follows: section 2 introduces the sea ice-ocean model and the snow scheme, section 3 details the experimental setup, and section 4 describes the observations used to evaluate the model outputs. In sections 5–6, we respectively present and discuss the mean state and variability of the sea ice extent/thickness for each simulation. Findings are summarized in section 7.

2. Model Description

[5] For the purpose of this study, we use the global coupled ocean-sea ice model NEMO-LIM, in the same configuration as in *Massonnet et al.* [2011]. Both the ocean-sea ice model and snow scheme we use are described in the next two sections.

2.1. Sea Ice and Ocean

[6] LIM3 (Louvain-la-Neuve Sea Ice Model, version 3) is a state-of-the-art thermodynamic-dynamic sea ice model. Its comprehensive description is given in *Vancoppenolle et al.* [2009a]. This model includes an explicit representation of the subgrid-scale distributions of ice thickness, enthalpy, salinity, and age (using five ice categories). The thermodynamic component is a multilayer

scheme (five layers of ice) based on the energy-conserving model of *Bitz and Lipscomb* [1999] and sea ice halodynamics are represented using an empirical parameterization of the effects of brine convection (gravity drainage) and percolation (flushing and snow ice formation) on the vertical salinity profile. Sea ice dynamics are solved using the elastic-viscous-plastic (EVP) rheology of *Hunke and Dukowicz* [1997] and the C-grid formulation of *Bouillon et al.* [2009]

[7] LIM3 is fully coupled with the oceanic general circulation model (GCM) OPA (Ocean PArallelisé, version 9) (see, *Madec* [2008] for the full documentation) on the modeling platform NEMO (Nucleus for European Modeling of the Ocean) following the formulation of *Goosse and Fichefet* [1999]. All simulations are performed on the model global tripolar ORCA1 grid (1° resolution) with 42 vertical levels. A sea surface salinity restoring toward the *Levitus* [1998] climatological values is added to the freshwater budget equation to prevent spurious model drift.

2.2. Snow Scheme
2.2.1. General Description

[8] Initially, the snow in LIM3 was, as in most ice-ocean GCMs, represented as one single layer with constant thermophysical properties. From this starting point, two general lines of model improvement were considered. The first is the sophistication of the physical and numerical framework used for snow representation (e.g., increasing the number of layers, introducing varying density, etc.), which is a prerequisite for parameterizing important processes such as penetration of shortwave radiation, snow packing and drift. The second line of improvement, i.e., the representation of the latter processes themselves, is partially addressed in this study and will be further developed in future studies. Thus, a multilayer thermodynamic snow scheme of intermediate complexity was developed and tested in the one-dimensional (1-D) version of LIM (LIM1D) [*Lecomte et al.*, 2011]. This scheme was then modified and included into the full version of NEMO-LIM3 for the present work in order to add a slightly improved radiation scheme, a new snow thermal conductivity formulation, and make it consistent with the structure of a three-dimensional model with horizontal advection. The final scheme, described hereafter, therefore provides a better characterization of the snow layer properties (density and thermal conductivity) and of their impacts on heat conduction through the snow ice system, compared to the initial snow representation in LIM3.

[9] For each sea ice thickness category in a given horizontal grid cell of the model, snow is considered as a horizontally uniform snow pack on sea ice, with a thickness h_s. At each depth z within the snow, the thermodynamic state of the medium is characterized by temperature $T(z)$, density $\rho_s(z)$, and effective thermal conductivity $k_{app}(z)$. The vertical snow temperature profile is governed by the one-dimensional heat diffusion equation:

$$c_s \rho_s \frac{\partial T}{\partial t} = \frac{\partial}{\partial z}\left(k_{app}\frac{\partial T}{\partial z}\right) - \frac{\partial I(z)}{\partial z} \qquad (1)$$

where $c_s = 2100$ J kg^{-1} K^{-1}, ρ_s, and k_{app} are the specific heat, density (handled as described in section 2.2.2.1), and thermal conductivity of snow (parameterized as a function of either density or wind speed, as detailed in section 2.2.2.2), respectively. $I(z)$ is the solar radiation penetrating into snow at depth z. Practically, the downwelling radiation decreases exponentially through the snow, except in its highly scattering uppermost portion [*Perovich*, 2007]. This layer is usually referred to as the "surface scattering layer" (SSL). In the new radiative scheme, we assume that the surface layer absorbs all near-infrared solar radiation [*Dozier and Warren*, 1982; *Warren*, 1982], so that the remaining radiation is in the visible and UV parts of the solar spectrum. Therefore, the snow column is optically divided into a highly scattering surface layer of thickness h_{SSL} and several deeper layers. The solar radiation penetrating under the SSL is:

$$I_0 = (1-\alpha)i_0 F^{sw}, \qquad (2)$$

where α is the surface albedo, F^{sw} the incident solar radiation at the surface, and $i_0 = 0.18$ the fraction of solar radiation penetrating under the SSL (value of *Grenfell and Maykut* [1977]). The albedo is computed as a function of the surface state, cloud cover, ice thickness, and snow depth [*Shine and Henderson-Sellers*, 1985]. Radiation transmission through the deeper layers is then computed following Beer's law, using a set of extinction coefficients κ_s for dry and wet snow from *Järvinen and Lepparanta* [2011]:

$$I(z) = I_0 e^{-\kappa_s z}, \qquad (3)$$

where $z > h_{SSL}$ is the snow depth. The parameter h_{SSL} is assigned to 3 cm (value of *Perovich* [2007]). Radiation absorption into the ice is also treated using Beer's law, with an attenuation coefficient $\kappa_i = 1$ m^{-1}. The crude representation of the radiative transfer in snow and sea ice should definitely be improved, for instance through the use of more sophisticated schemes [e.g., *Briegleb and Light*, 2007; *Holland et al.*, 2012], which will be the subject of future work.

[10] The surface energy balance provides the boundary condition at the top of the snow cover (fluxes are defined positive downward):

$$F_0^{ct} = (1-\alpha)(1-I_0)F^{sw} + F^{lw} - \epsilon_s \sigma T_s^4 + F^{sh} + F^{lh} \qquad (4)$$

[11] F_0^{ct} being the conductive heat flux in snow just below the surface, F^{lw} the downward longwave radiation, $\epsilon_s = 0.97$ and T_s the surface emissivity and temperature, respectively, and F^{sh} and F^{lh} the turbulent fluxes of sensible and latent heat. In LIM3, the heat content of three snow physical layers and the total snow mass (per ice category) are advected horizontally with the sea ice, as suggested by *Lecomte et al.* [2011]. This minimum

number of layers was chosen to avoid an excessive increase in computing time, closely related to the number of state variables advected in the model. Considering that no optimization of the code was done at this stage, this configuration leads to a lengthening of the actual computing time by ~40% compared to the standard version of NEMO-LIM3 with a single snow layer. Most of this cost is due to the advection of snow mass and temperature tracers (20 tracers) using the Prather scheme, the cost of which significantly increases with a large number of tracers. However, the snow vertical grid is refined in The thermodynamics so that the heat diffusion equation is solved within six layers instead. This is done using an energy-conserving method and enables the thermodynamic scheme to better simulate the temperature gradient within the snow cover.

[12] Once the new temperatures are computed, the snow mass balance is calculated as:

$$\frac{\partial M_s}{\partial t} = R_S - R_{M/Su} - R_{SI} \qquad (5)$$

where M_s is the snow mass per unit area (integral of snow thickness times density over all layers), R_S the snowfall rate, $R_{M/Su}$ the melt or sublimation rate, and R_{SI} the snow ice formation rate. $R_{M/Su}$ accounts for both surface and internal melts, and surface sublimation whenever the snow surface specific humidity is larger than the air specific humidity. Basically, when the surface energy balance is positive for snow (taking into account all incoming and outcoming fluxes) and surface temperature reaches the melting point, snow melts. If the snow surface specific humidity (relative to the temperature of the surface layer) is larger than the air specific humidity and the air relative humidity is lower than 100%, snow sublimates instead of melting. Since the energy by unit mass required to sublimate snow is about 10 times larger than the one for melting it, snow mass losses by surface ablation in case of sublimation are significantly reduced compared to regular melt conditions [*Nicolaus et al.*, 2009].

[13] R_{SI} is parameterized as in *Fichefet and Morales Maqueda* [1997]. When the snow pack is heavy enough to depress the snow-ice interface below the sea level, a mixture of snow and sea water flooding the interface refreezes to form snow ice that is merged with the underlying sea ice. The thickness of the snow ice layer is computed assuming the hydrostatic equilibrium of the snow/ice column into the ocean.

[14] The snowfall rate, R_S is initially derived from climatological data, as a surfacic water mass flux (in kg m^{-2} s^{-1}). Then, R_S is converted into snow accumulation Δh^{sfall}:

$$\Delta h^{sfall} = f^{sfall} \rho_s f^{solid} R_S \Delta t \qquad (6)$$

where f^{solid}, f^{sfall}, and Δt are the fraction of precipitation that falls as snow, the fraction of solid precipitation falling on the ice-covered part of the grid cell and the model time step, respectively. f^{solid} is computed as a

function of surface air temperature following *Ledley* [1985], and f^{sfall} is defined as

$$f^{sfall} = \frac{1-(1-a_i)^{\beta}}{a_i} \qquad (7)$$

where a_i is the ice concentration (area fraction) and β a blowing snow parameter (equal to 0.6 in the model) accounting for the impact of the wind on the amount of snow blown into the ocean.

2.2.2. Parameterizations
2.2.2.1. Snow Density Profile

[15] The representation of snow metamorphism in a model, implying the characterization of the snow pack through the snow grain size and shape, requires a high level of sophistication that is not compatible with both the spatial scales resolved explicitly by GCMs and the computational costs of such models. Despite being beneficial for the representation of some processes, such as the physics of depth hoar formation [see, e.g., *Sturm and Massom*, 2009], a comprehensive description of metamorphism like the one used in complex land snow models (e.g., CROCUS [*Brun et al.*, 1989]) was not included in LIM3. Besides, in contrast with the density of continental snow, the density of snow on sea ice is affected by sea ice dynamics and topography.

[16] Nonetheless, the impacts of such mechanisms on snow are so poorly understood that prognosing the evolution of snow density in a sea ice model is hardly feasible at this stage. Instead, a density profile is prescribed as a function of the sea ice age and thickness, and only the snow mass (not volume) is advected on the horizontal grid of the model. This is done by assuming that the snow depth and stratigraphy are highly conditioned by the history of the underlying sea ice. Studies presenting specific snow stratigraphies on first-year ice (FYI) and multiyear ice (MYI), such as *Nicolaus et al.* [2009], support this assumption. Two main observational data sets were used to build the snow density profiles for FYI and MYI in the model. The first is from the interdisciplinary Ice Station POLarstern (ISPOL) [*Hellmer et al.*, 2008] project, Weddell Sea, Antarctica. The campaign was conducted in the western Weddell Sea, Southern Ocean in austral spring and summer 2004/2005. Regular measurements (over December 2004) of snow density profiles were made in four sites including both FYI and MYI around the drifting station. A full description of these data can be found in *Nicolaus et al.* [2006] and *Nicolaus et al.* [2009]. In the Arctic, snow density data were taken from the Canadian Arctic Shelf Exchange Study (CASES) that took place in 2003. This data set, described in *Langlois et al.* [2007], provides snow density profiles on first-year land-fast sea ice offshore in Franklin Bay, Northwest Territories, Canada.

[17] First, those snow pit data were processed to bring all densities and layer thicknesses back on a normalized vertical grid with depth $\hat{z}$ varying from 0 (surface) to 1 (bottom). The normalized density profiles were then averaged over snow samples originating from sea ice of similar type and thickness. From this, a uniform snow density profile of 290 kg m^{-3} and a vertical profile $\rho_s(\hat{z})=291+89\hat{z}$ [kg m^{-3}] were chosen to be prescribed in the model for snow on FYI and MYI, respectively. Given the very high spatial (even at regional scale) and temporal variability of the snow cover on top of sea ice in both hemispheres [e.g., *Massom et al.*, 2001; *Sturm et al.*, 2002], this modeling choice might appear relatively simple. However, it is a first attempt to account for the impact of the variability of the snow stratigraphy on the large-scale sea ice thermodynamics. In the context of the multiplication of snow in situ data sources, this method could be refined to add more detailed and distinct profiles as a function of ice type in large-scale sea ice models.

2.2.2.2. Snow Thermal Conductivity

[18] The snow thermal conductivity is usually related to snow density through data regressions. Here, we use those of *Yen* [1981] (equation (8)) and *Sturm et al.* [1997] (equation (9)):

$$k_{app} = k_i \left(\frac{\rho_s}{\rho_w} \right)^{1.88} \qquad (8)$$

$$k_{app} = 0.138 - 0.00101\rho_s + 0.000003233\rho_s^2 \qquad (9)$$

with k_i and ρ_w being the thermal conductivity of pure ice (2.01 W K^{-1} m^{-1}) and the density of freshwater (1000 kg m^{-3}), respectively. Those relationships were chosen in *Lecomte et al.* [2011] because they are broadly used in the snow-modeling community. However, due to the dissimilar meteorological conditions, sea ice types and thickness distributions in the two hemispheres, the Arctic and Antarctic sea ice snow cover properties (in particular density stratigraphy) are substantially different [*Sturm and Massom*, 2009]. In light of the current state of snow representation in sea ice models, these differences cannot be well represented yet. The evaluation of snow thermal conductivity based on such relationships is therefore critical and sometimes leads to large errors in thermal conductivity (and subsequently in sea ice state estimates) according to whether they are used in the Northern or Southern Hemisphere. For these reasons, we have sought to develop simple parameterizations of snow density and thermal conductivity that would be independent from those considerations and would directly relate the snow density and thermal conductivity to climate variables such as the surface wind speed, the surface air temperature or the temperature gradient in the snowpack. Here, we briefly present the correlations obtained in [*Domine et al.*, 2011b] between the snow density and the mean seasonal surface wind speed and between the snow thermal conductivity and the mean seasonal surface wind speed ($\overline{w}$). The rationale is the observation, common and shared by virtually all field snow scientists, that the hardness and density of dry snow are largely determined by the wind intensity. This widespread observation has been published and used in continental snow models [e.g., *Brun et al.*, 1997; *Vionnet et al.*, 2012] but, to the best of our knowledge,
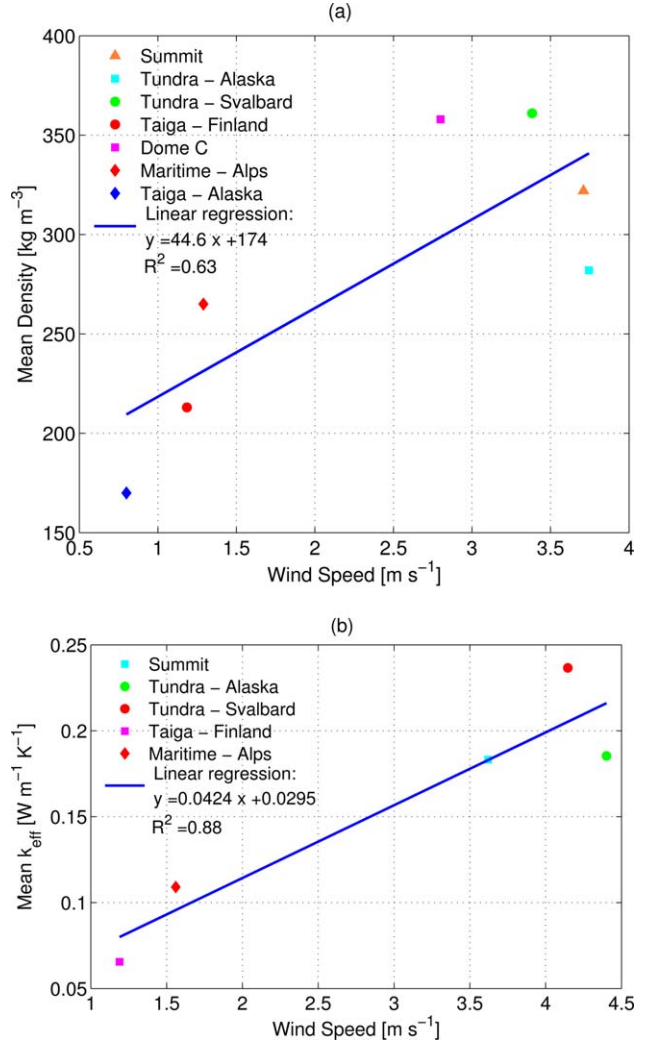
never in sea ice models. Since both snow hardness and density are good predictors of the snow thermal conductivity [*Domine et al.*, 2011a], relating this latter variable to the surface wind speed also appears logical.

[19] We used data from field campaigns in Sodankylä (Northern Finland), Barrow (Alaska) [*Domine et al.*, 2012], the Col de Porte (French Alps), Ny Alesund (Svalbard) [*Domine et al.*, 2011a], and Summit (Greenland) for thermal conductivity. For density, in addition to the aforementioned locations, we used data from Fairbanks (Alaska) [*Taillandier et al.*, 2006] and Dome C (Antarctica). The data from places with references have been published, and most of the others have been obtained for a purpose totally different from that of the current study. Data from Col de Porte, Summit, and Dome C have not been published yet. As detailed in *Domine et al.* [2012], the snow density was measured with density cutters, i.e., by extracting and weighting a known volume of snow. The snow thermal conductivity was measured with a TP02 heated needle probe from Hukseflux. The principle is to measure the rate of dissipation of a 100 s heat pulse by monitoring the temperature rise of the heated needle [*Sturm et al.*, 1997; *Morin et al.*, 2010]. This rate is related to snow thermal conductivity. Meteorological data was either measured during the campaigns or taken from permanent meteorological stations at the sites. The temperature gradient within the snow was determined from vertical strings of thermistors placed in the snow during the campaign. The site of Sodankylä is in the forest and wind speed is measured above the canopy. This is clearly not representative of wind speed at ground level. At this site, essentially no wind could be felt at ground level and there was never any blowing snow. These conditions were similar to those experienced in Fairbanks, so that the wind speed above the canopy was scaled to the ratio between the wind speeds above and below the canopy from Fairbanks to obtain the below canopy Sodankylä wind speed.

[20] The correlation between the snow density and the surface wind speed is shown in Figure 1 (left). In this figure, the surface wind speed is the seasonal one. The snow density is the average of all density data over a season, as in the case of Fairbanks, or over the campaign duration, which ranges from 2.5 months (Summit) to 3 weeks (Finland). These data lead to the following relationship:

$$\rho_s = 44.6\overline{w} + 174 \left(\text{kg m}^{-3}\right) \qquad (10)$$

[21] The associated correlation coefficient $R^2 = 0.63$, based on seven samples, is statistically significant ($p \leq 0.05$). It can be enhanced by adding a temperature gradient component. The rationale is that the temperature gradient tends to reduce the density in seasonal snowpacks, where the warmer basal layers sublimate and lose mass while not compacting [*Sturm and Benson*, 1997; *Taillandier et al.*, 2006]. Empirically, we found that $\rho_s = \overline{w} - 0.13\nabla T$, with ∇T, in K m^{-1}, yielding the best correlation, $R^2 = 0.82$ ($p \leq 0.05$). However, computing the seasonal mean temperature gradient in the snowpack significantly increases the numerical memory requirements of the model, so that only the wind speed

(a)

(b)

Figure 1. Correlation between (a) the mean snow density/(b) thermal conductivity and the mean seasonal surface wind speed at various locations (see section 2.2.2.2 for details).
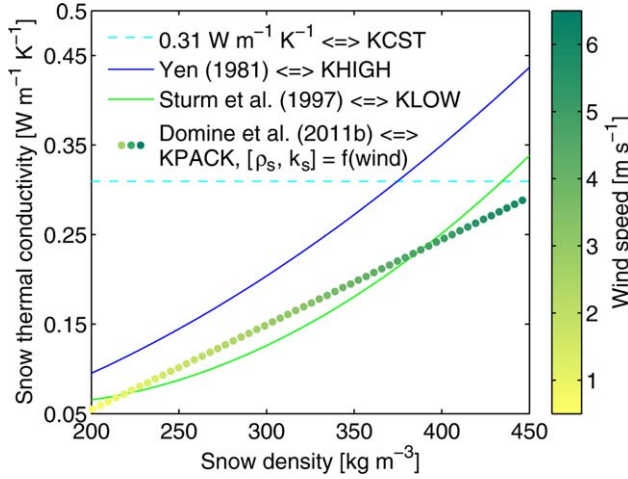
correlation was actually retained. The correlation between the snow thermal conductivity and the surface wind speed is illustrated in Figure 1 (right), and yielded the following regression:

$$k_{app} = 0.0424\overline{w} + 0.0295 \left(\text{Wm}^{-1}\text{K}^{-1}\right) \qquad (11)$$

[22] Based on five points, $R^2 = 0.88$ ($p \leq 0.05$). It can be enhanced to 0.91 ($p \leq 0.05$) by adding a temperature gradient component but for the same reasons as above, this was not implemented in the model. Second-order polynomial fits were also applied to these data but were not statistically significant for snow density as a function of wind speed, so they were not retained.

2.2.2.3. Basic Intercomparison

[23] The constant value of 0.31 W m^{-1} K^{-1} usually used for k_{app} in sea ice models was historically taken from the formulation of *Abels* [1892] for snow of

Figure 2. Snow thermal conductivity versus density for *Yen* [1981] and *Sturm et al.* [1997] relationships. Colored dots of coordinates (ρ_s, k_s) represent snow thermal conductivity and density as functions of wind speed from *Domine* et al. [2011b].

density equal to 330 kg m^{-3}. As depicted in Figure 2, this value is greater than the thermal conductivities produced by all other relationships introduced above for low to medium densities, and especially for light snow. Equation (9) provides lower thermal conductivities than (8), because *Sturm et al.* [1997] studied depth hoar of subarctic taiga in large proportion. Since this snow type has the lowest k_{app}, this artificially decreased their values [*Domine et al.*, 2011a]. For this reason, the model simulations associated to formulations (8) and (9) in section 3.2 are named KHIGH and KLOW, respectively. The new regressions ((10) and (11)) lead to thermal conductivity values in between those of (8) and (9), for the usual range of snow densities in the model. Because regression 10 represents a simple parameterization of snow packing, the corresponding simulation is called KPACK in the following sections.

3. Model Forcing and Experimental Design

3.1. Forcing

[24] A combination of atmospheric reanalyses and climatologies are used to drive the sea ice-ocean model. We use the NCEP/NCAR daily reanalyses of 2 m air temperature and 10 m u- and v-wind components [*Kalnay et al.*, 1996], and monthly climatologies of relative humidity [*Trenberth et al.*, 1989], total cloudiness [*Berliand and Strokina*, 1980], and precipitation [*Large and Yeager*, 2004]. River runoff rates are derived from *Dai and Trenberth* [2002].

[25] All forcing fields are spatially interpolated from a $2° \times 2°$ latitude-longitude grid to the ORCA1 grid. Surface radiative and turbulent heat fluxes are calculated following *Goosse* [1997]. The surface wind stress over sea ice is computed with a quadratic bulk formula assuming a drag coefficient $C_a = 1.40 \times 10^{-3}$.

3.2. Model Setup and Simulations

[26] All simulations are run from 1948 to 2007, but the analysis and the comparison of model output with observations are made over the 1979–2007 period, for which satellite data are available. Initial ocean temperature and salinity fields are taken from *Levitus* [1998]. Wherever the sea surface temperature is below 0°C, sea ice thicknesses (snow depths) of 3.5 (0.3 m) and 1 m (0.1 m) are prescribed in the Arctic and the Southern Oceans, respectively. Ice concentration is initialized to 0.95 and 0.90 in the ice-covered regions of the Northern and Southern Hemispheres, respectively. Initial sea ice and snow temperatures are fixed to 270 K, and sea ice salinity to 6 PSU. The ocean model time step is $\Delta t_0 = 1$ h and the sea ice model is called every six ocean time steps.

[27] From the thermal conductivity and density formulations described in section 2.2.2.2., four simulations, hereafter referred to as KPACK, KCST, KHIGH, and KLOW, were performed. Table 1 makes explicit which parameterization was used in each run. The first simulation (KPACK) was carried out using equations (10) and (11). KCST was run utilizing a constant snow thermal conductivity (equal to 0.31 W m^{-1} K^{-1}) for each snow layer. KHIGH and KLOW were conducted using relationships (8) and (9), respectively, and prescribing the snow density profile as described in section 2.2.2.1.

4. Observations

[28] In the next sections, we assess the skill of all model simulations in both hemispheres by comparing their sea ice thicknesses, concentrations, and extent to observations coming from different sources.

[29] Two sets of observational data are used to validate the modeled ice thickness. In the Northern Hemisphere, draft data (defined as the ice thickness below sea level) measured by Upward Looking Sonars (ULS) onboard submarines are available from 1979 to 2000. These data, described in *Rothrock et al.* [2008], are provided by the NSIDC (National Snow and Ice Data Center). They include mean drafts from more than 3000, 50 km long transects and about 30 cruises. According to *Rothrock et al.* [2008], the ULS observational errors have a standard deviation of 0.38 m with no significant bias. In the Southern Ocean, we use the ASPeCt (Antarctic Sea Ice Processes and Climate) data of

Table 1. List of the Simulations Performed With the Model, Using the New Snow Scheme

Simulation Name	Parameterization Used for Snow Density and Thermal Conductivity
KPACK	Density and effective thermal conductivity of *Domine et al.* [2011b], equations (10) and (11).
KCST	Prescribed density (as detailed in section 2.2.2.1). Constant thermal conductivity = 0.31 W m^{-1} K^{-1}.
KHIGH	Prescribed density (as detailed in section 2.2.2.1). Effective thermal conductivity of *Yen* [1981].
KLOW	Prescribed density (as detailed in section 2.2.2.1). Effective thermal conductivity of *Sturm et al.* [1997].

Table 2. Mean Absolute Value of the Difference Between Observed and Simulated Variables[a]

		KPACK	KCST	KHIGH	KLOW
Mean thickness	NH (Draft)	*0.63*	1.08	0.64	1.55
error (m)	SH	0.36	0.36	0.35	*0.34*
	(Thickness)				
Mean extent	NH	*0.35*	0.44	0.40	1.00
error (10^6 km^2)	SH	1.01	1.06	0.92	*0.72*
Ext. Ano.[b] trend	NH	0.027	0.032	0.030	*0.013*
error (10^6 km^2/yr)	SH	0.012	0.013	0.008	*0.005*
Ext. Ano.[b] std	NH	0.16	0.21	0.19	*0.005*
error (10^6 km^2)	SH	0.14	0.16	0.12	*0.07*

[a]For draft and thickness errors, the average of the difference mod.—obs. (in absolute value) is computed over all observation locations. For sea ice extent, the mean annual cycle over 1979–2007 is computed for the model and the observations, and the annual mean of the difference between the two (in absolute value) is calculated. Observed and simulated monthly extent anomalies are retrieved with respect to the mean annual cycles of sea ice extent, in order to compute their trends and standard deviations over 1979–2007. The same method (absolute value of the difference mod.—obs.) is then applied to the latter quantities to get the errors. The best statistics for each diagnostic are enhanced using italics font.

[b]"Ext. Ano." stands for extent anomaly.

Worby et al. [2008a], which consists of about 14,000 estimates of sea ice thickness over the 1983–2000 period. Sea ice thicknesses from this data set are observed from ships when they break the ice and turn it sideways. Errors in the ASPeCt thickness range from $\pm 20\%$ to $\pm 30\%$ for undeformed and deformed ice, respectively [*Worby et al.*, 2008a; *Kurtz and Markus*, 2012].

[30] For ice concentration, we use in both hemispheres the data from the Scanning Multichannel Microwave Radiometer (SMMR) and the Special Sensor Microwave/Imager (SSM/I) reprocessed by the *EUMETSAT Ocean and Sea Ice Satellite Application Facility* (*Tonboe and Nielsen*, 2010), from 1983 to 2007. The data were interpolated onto the model grid in order to perform the pointwise comparison with the simulated sea ice concentrations. Sea ice extent is then computed based on monthly fields of ice concentration from both model runs and satellite data, as the total area of oceanic grid cells covered by more than 15% of sea ice.

[31] Finally, we qualitatively compare the model snow depth distributions to those obtained by *Kwok et al.* [2011] and *Kurtz and Farrell* [2011], from large-scale airborne surveys over the Arctic basin, and by *Worby et al.* [2008b], who evaluated the EOS Aqua Advanced Microwave Scanning Radiometer (AMSR-E) snow depth product in the Southern Ocean.

5. Results

[32] In the following, we discuss the model ability to simulate the mean state and variability of the Arctic and Antarctic sea ice covers over the 1979–2007 period. All deviations between observed and simulated quantities are expressed in terms of absolute value of the difference model—observation. Absolute values were chosen to avoid compensation of deviations with opposite signs, and resulting in misleading small values. A summary of these errors is given in Table 2.

5.1. Mean State

[33] We invite the reader to refer to Figures 3 and 4 together with Table 2. Figure 3 shows the mean seasonal cycles of sea ice extent in both hemispheres, for all simulations and as observed. Figure 4 displays the differences between the simulated and observed sea ice drafts in the Northern Hemisphere at places where observations are available. Red (blue) areas show where the model overestimates (underestimates) the sea ice draft or thickness. The equivalent maps are not shown for the Southern Hemisphere for reasons that are given in section 5.2.2. The mean snow state is illustrated in Figure 5, which shows the April mean Snow Depth Distribution (SDD) averaged over the last decade of each run on both Arctic FYI and MYI (we use the category-averaged snow depths to compute them), while Figure 6 depicts the Antarctic annual mean snow depths over sea ice for each simulation.
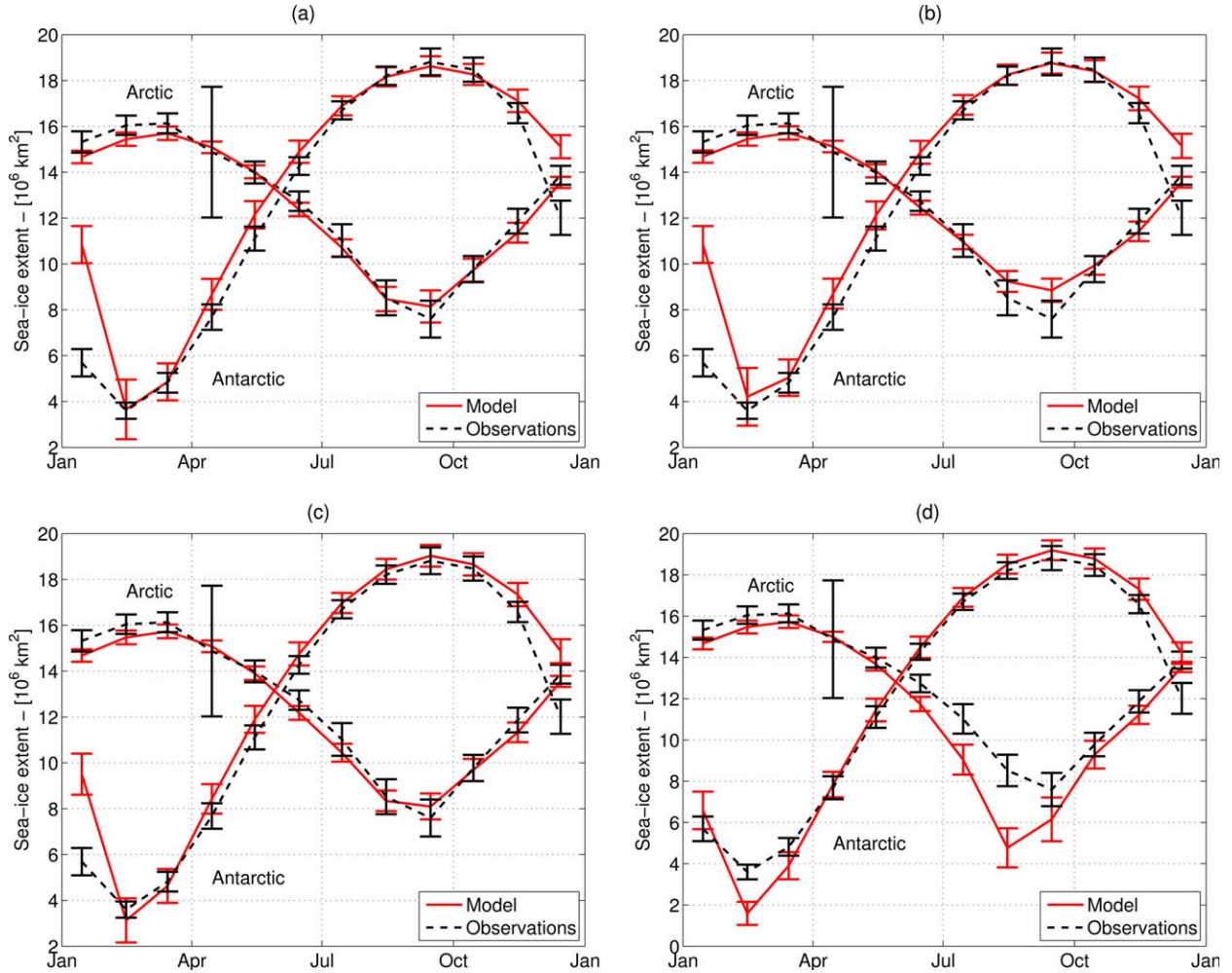
5.1.1. Northern Hemisphere

[34] As shown by Figures 3 and 4, KPACK and KHIGH both provide a realistic mean sea ice state in the NH. For KPACK, the sea ice extent annual mean deviation and the draft mean absolute error with respect to observations are 0.35×10^6 km^2 (2.8%) and 0.63 m, respectively. The mean draft in this simulation is overestimated by 2.3%. With such errors, typical for NEMO-LIM3 in the ORCA1 configuration [*Massonnet et al.*, 2011], both globally and regionally, KPACK exhibits the best skill in simulating the Arctic sea ice extent and thickness among all simulations. KHIGH has slightly larger sea ice extent and draft mean errors (0.4×10^6 km^2 and 0.64 m). KCST and KLOW overestimate and underestimate the mean sea ice draft, with relative errors of $+34.5\%$ and -53.3%, respectively. KLOW presents by far the largest ice extent absolute differences with observations, with a mean value reaching 1.0×10^6 km^2 ($\sim 10\%$).

[35] All model simulations do reasonably well in reproducing the observed SDD in the Arctic. In all cases, the snow depth on FYI ranges from 0 to 45 cm, with a peak at 10 cm (instead of 15 cm in *Kwok et al.* [2011]) in the SDD. On MYI, the maximum snow depth is about 120 cm for KCST, KHIGH, and KLOW (peak in SDD around 45–50 cm), while it is only 100 cm for KPACK (peak at 30 cm). With mean snow depths (over 1997–2007) varying from 7 (15 cm) to 17 cm (31 cm) on FYI (MYI), the snow pack appears globally too thin but the shape and width of the SDDs are relatively well captured given the possible errors in the precipitation climatology used to force the model, especially in KPACK.

5.1.2. Southern Hemisphere

[36] As revealed by Table 2, the model sea ice thickness is less sensitive to the snow thermal conductivity in the SH than in the NH. A similar mean error of about 35 cm is found for all runs, which explains why maps equivalent to those displayed in Figure 4 are not shown for the SH. In contrast, Figure 3 indicates that the SH

Figure 3. Simulated and observed (*Tonboe and Nielsen*, 2010) mean seasonal cycle of sea ice extent over the period 1979–2007, for simulations (a) KPACK, (b) KCST, (c) KHIGH, and (d) KLOW. Extents are calculated as the total area of oceanic grid cells with ice concentration larger than 15%. The error bars denote the standard deviation of monthly extents during the period of analysis.

sea ice extent is relatively sensitive to the snow thermal conductivity formulation. While KLOW is relatively poor in the Arctic, it performs better in the SH with respect to ice extent (error of 0.72×10^6 km^2, i.e., 10.5%) than the other runs ($\sim 1.0 \times 10^6$ km^2). The model tends to underestimate the SH mean sea ice thickness by $\sim 30\%$, compared to the ASPeCt ice thickness product. In *Fichefet et al.* [2000], a negative ice-ocean feedback was detected when reducing the snow thermal conductivity, with less ice growth and therefore less brine rejection, in turn resulting in weaker oceanic heat fluxes to the ice due to the stronger ocean stratification. In their study, the latter process triggered an enhanced sea ice thermodynamic production competing with, and sometimes compensating, the initial drop in sea ice growth rate. Such a feedback is not clearly observed here, probably because some of the model components are substantially different. In particular, NEMO-LIM3 includes the sea ice thickness distributions, a prognostic salinity, a treatment of the vertical mixing in the ocean different from the one in the ocean

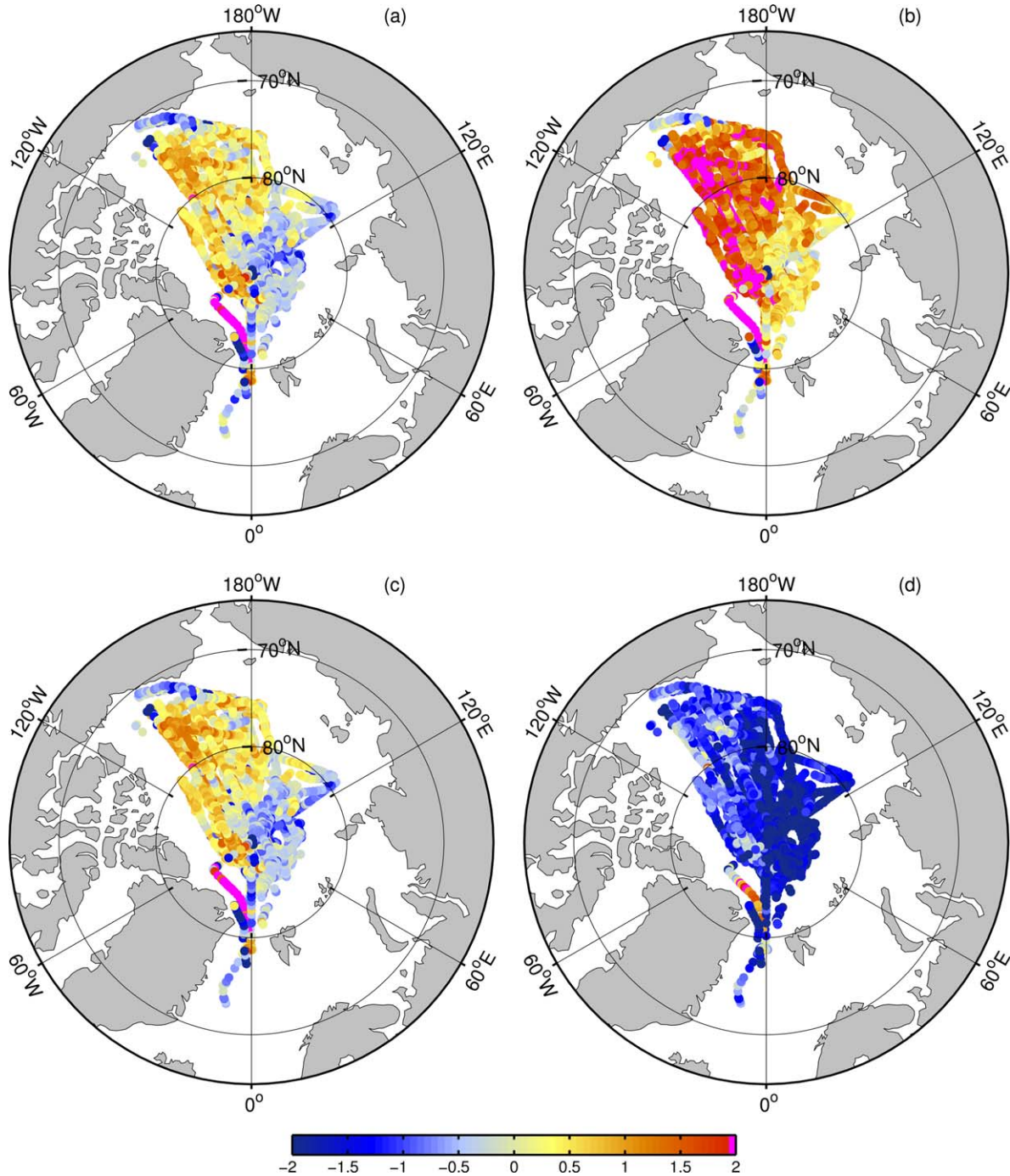model of *Fichefet et al.* [2000], and was used at a higher resolution.

[37] A common problem of all model runs is their inability to reproduce the fast decrease in extent in November-December (see Figure 3). This typical feature for the NEMO-LIM3 ORCA1 configuration of the model was already observed in *Massonnet et al.* [2011] and is still unexplained.

[38] As in the NH, although the observed geographical distribution of snow depth is reasonably well reproduced, in particular with regards to the ASPeCt snow data, the model tends to underestimate the snow depths compared to the Advanced Microwave Scanning Radiometer (AMSR-E) snow depth product [*Worby et al.*, 2008b] (not shown). The maximum snow depth is found in the Weddell Sea and reaches 25 cm in KCST, against 19 cm only in KPACK.

5.2. Variability

[39] Surprisingly, the simulations yielding the best estimates for mean state are not necessarily those
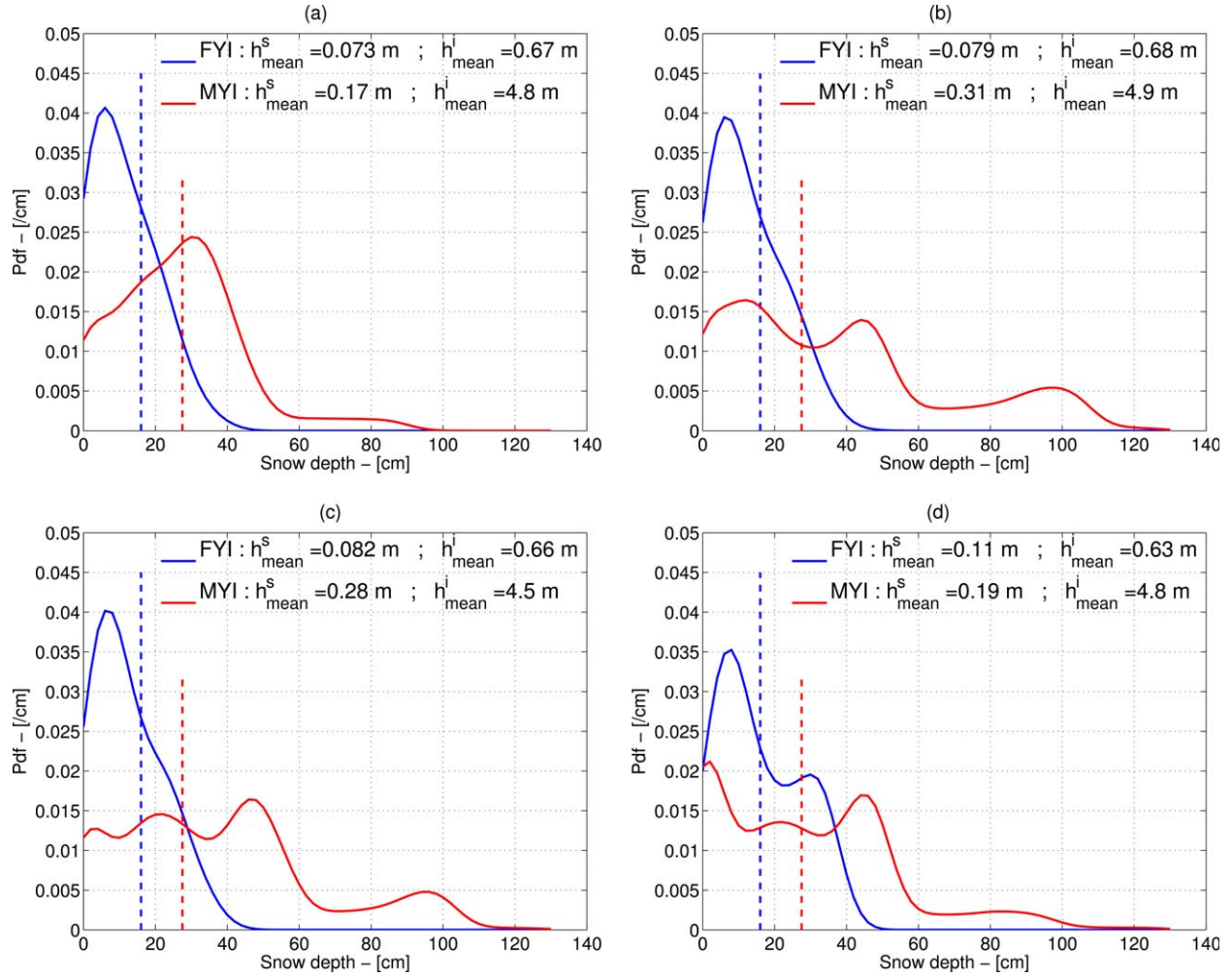
Figure 4. Differences (in meters) between simulated and ULS (National Snow and Ice Data Center, 1998, updated 2006) sea ice drafts in the Northern Hemisphere (mod.—obs.), for simulations (a) KPACK, (b) KCST, (c) KHIGH, and (d) KLOW. Modeled drafts have been chosen according to the month and year of the observation. The corresponding grid cell has been chosen as the closest to the coordinates of the observation.

providing the ice extent anomalies in best agreement with observations. Figure 7 shows the time series and trends of the monthly anomalies in sea ice extent in both hemispheres through 1979–2007 for KPACK and KLOW. Because they are qualitatively similar, we only show these plots for KPACK, and compiled the statistics for the other runs in Table 2. Both Figure 7 and Table 2 reveal that KLOW systematically outperforms all other runs in reproducing the observed sea ice extent anomalies, with relative errors of −25.3% (−23.1%) for the trend in extent anomaly and +0.8% (+13.3%) for the standard deviation in extent anomaly

Figure 5. Arctic mean snow depth probability density functions (1997–2007) on FYI and MYI for simulations (a) KPACK, (b) KCST, (c) KHIGH, and (d) KLOW. Category-averaged snow depths are used to compute the distributions. Vertical dashed lines represent the modal snow depth from *Kwok et al.* [2011], for FYI (blue) and MYI (red).

in the NH (SH). Contrary to the mean sea ice state, the sea ice variability seems to be equally sensitive to the snow thermal conductivity formulation in both hemispheres.
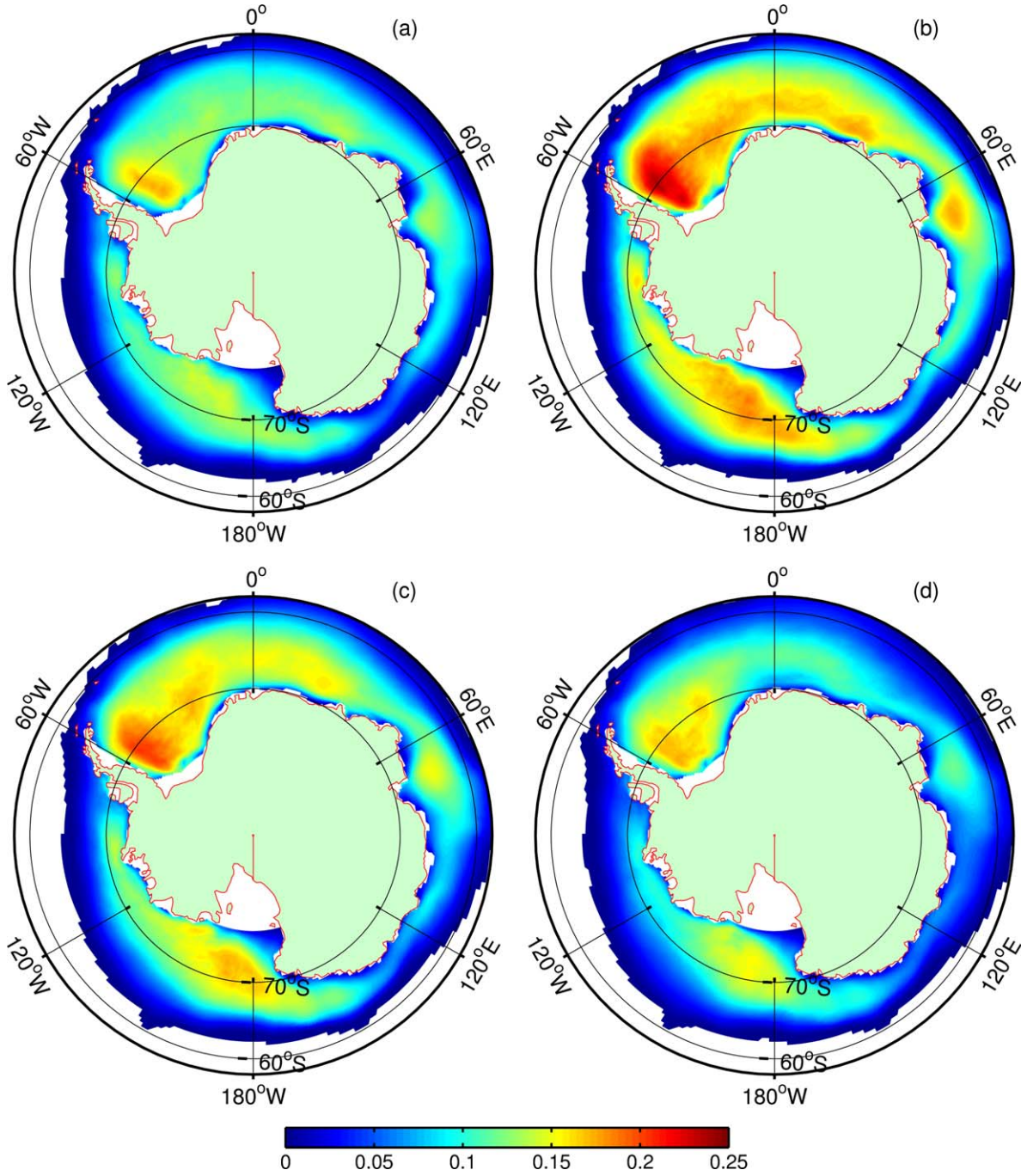
6. Discussion

6.1. Mean State

[40] As shown in section 5.1, KCST overestimates the Arctic sea ice volume while such a behavior was not observed with the former representation of snow in the model [see, e.g., *Vancoppenolle et al.*, 2009a]. Two reasons can be invoked. First, as explained in section 2.2.2.3., the snow thermal conductivity in KCST seems to be overestimated compared with other formulations, particularly for snow on FYI that has smaller densities in the model. The result is a strongly enhanced FYI growth rate in winter. Second, our snow scheme is multilayered and better resolves the vertical temperature profile in the snow, making the model more sensitive to the surface thermodynamic

forcing compared to its former version. This feature is also observed in the Southern Ocean, although less significantly. As clearly shown by Figure 8, presenting the seasonal cycle of the sea ice mass balance spatially integrated terms, the surface energy budget in the Southern Ocean is such that it rarely leads to surface melt. Hence, the sea ice mass balance in the South is rather driven by snow ice formation, and formation and melting at the base. Therefore, the relative importance of atmospheric processes is likely smaller than in the Arctic. Compared to KCST or KPACK, KLOW produces more insulating snow on top of sea ice that curtails the heat loss from the ice to the atmosphere and thus limits the basal ice growth in winter (see Figure 8). FYI therefore covers a larger part of the Arctic Ocean during wintertime, in turn leading to a significantly reduced sea ice summer extent. Among all simulations, KHIGH leads to the most realistic sea ice thicknesses with a snow thermal conductivity relationship naturally leading to values widely varying between those produced by KLOW and KCST.
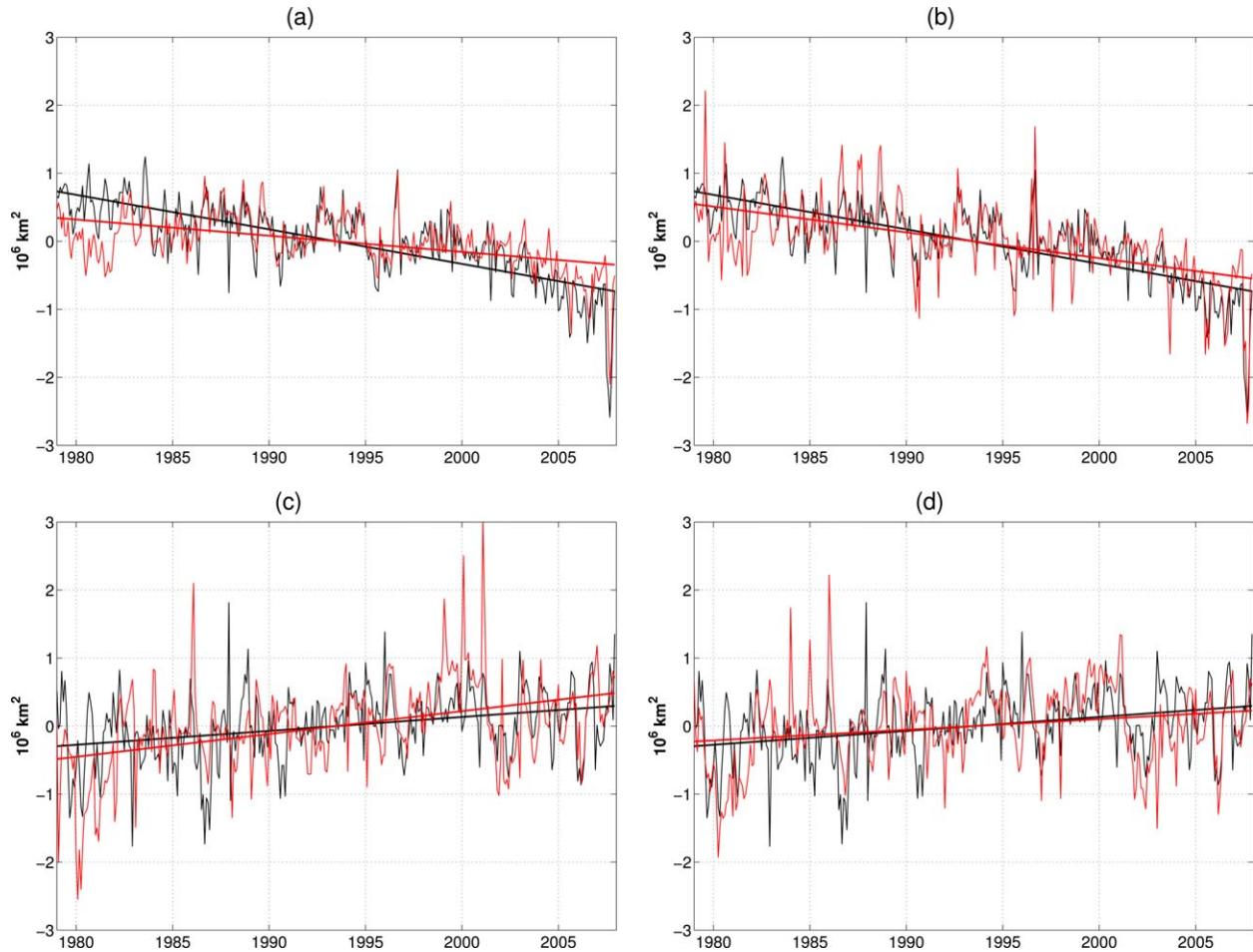
Figure 6. Antarctic annual mean snow depths (1997–2007; in meters) for simulations (a) KPACK, (b) KCST, (c) KHIGH, and (d) KLOW.

[41] The Arctic sea ice draft simulated by the KPACK and KLOW runs differ substantially from each other, as depicted in Figure 4. Yet, the snow thermal conductivities for these two parameterizations look similar (Figure 2). To explain this apparent contradiction, we put forward two reasons. First, the snow thermal conductivity in KPACK is a function of the wind speed only, and the winds from the atmospheric forcing are large ($\sim$5–10 m s^{-1}). For this simulation, k_{app} reaches values at the upper tail of the distribution, say

$\sim$0.3 W m^{-1} K^{-1}. In the KLOW run, k_{app} is a function of snow density only ($\sim$300 kg m^{-3} in the model), thus reaching lower values and limiting ice growth in winter. Second, snow density is also a function of wind speed in the KPACK simulation, and for the same reasons it is higher on average than the KLOW density. For the same snow mass, the snow cover will accordingly be thinner in KPACK (see also top left of Figure 5), thus enhancing heat transfers compared to KLOW. These two effects add up to produce a thicker ice in KPACK

Figure 7. Simulated (red) and observed (black) (*Tonboe and Nielsen*, 2010) monthly anomalies in sea ice extent (relative to the mean seasonal cycle of sea ice extent) in the (top) NH and (bottom) SH over the period 1979–2007, for (a) KPACK Arctic, (b) KLOW Arctic, (c) KPACK Antarctic, and (d) KLOW Antarctic. The plain lines indicate the trends computed from linear regression over the same period.
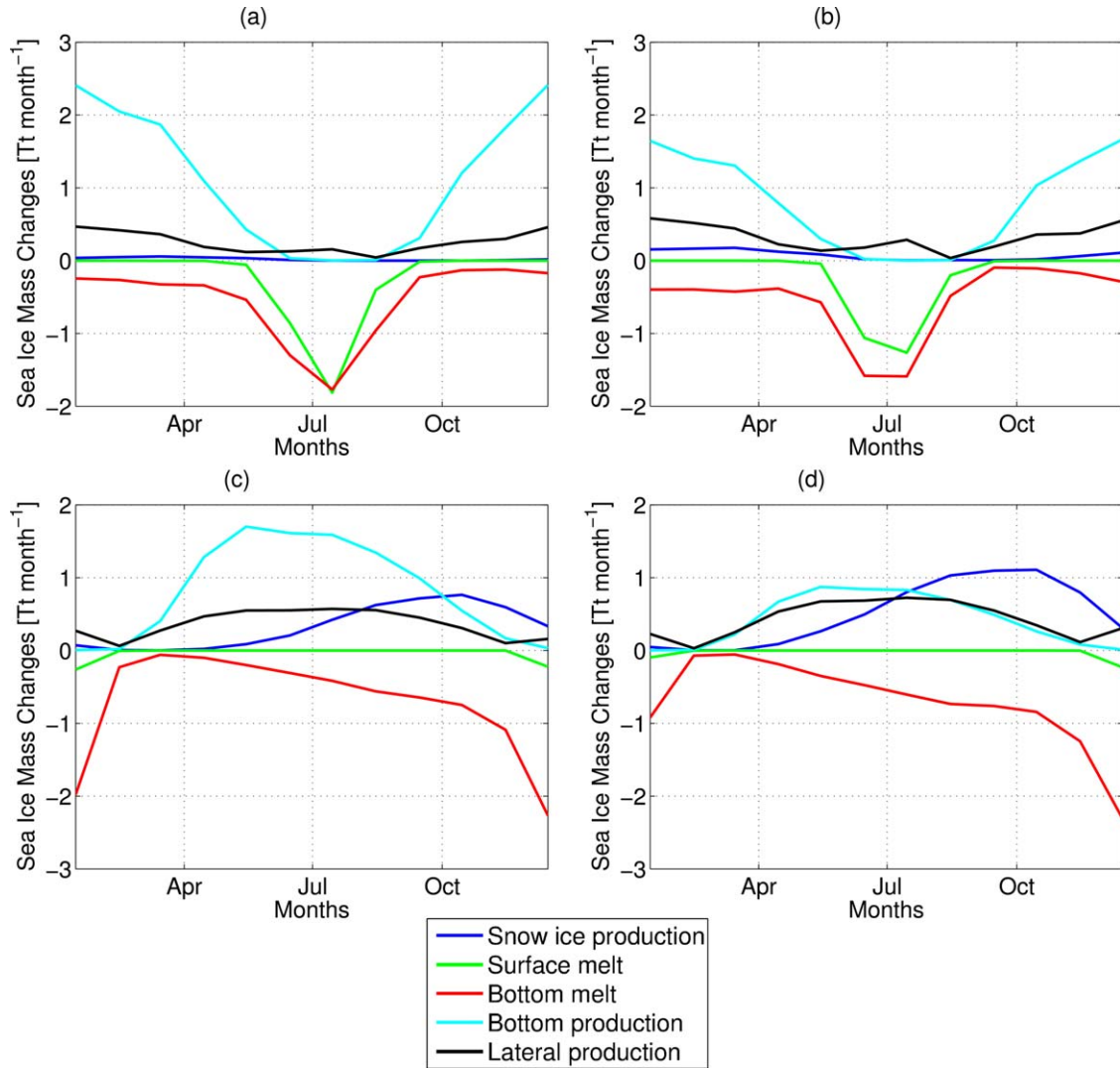
than in KLOW, and explain the significant difference in sea ice bottom production between the two simulations (Figure 8).

[42] In all simulations and in both hemispheres, the sea ice thickness and extent are also considerably sensitive to the SDDs. Although qualitatively those distributions seem to be rather well reproduced, quantitatively the observed SDDs of *Kurtz and Farrell* [2011] or *Kwok et al.* [2011] as well as the geographical distribution of mean snow depth in the Southern Ocean are not captured. Errors can be attributed to the forcing or to the model itself. Regarding the forcing, using a climatology for precipitation involves the loss of interannual variability. Besides, the atmospheric reanalyses and climatologies used to force the model have known biases [e.g., *Bromwich et al.*, 2007; *Vancoppenolle et al.*, 2011]. In particular, a bias in snow precipitation is likely to affect the simulated SDDs by shifting them toward thicker or thinner snow, thus improving or worsening the quantitative comparison with observed SDDs, respectively. Interestingly, KPACK provides the best distribution shapes compared to the observational stud-

ies mentioned previously. This simulation uses regression (8), which emphasizes the importance of accounting for the direct influence of wind on snow depth, and ultimately suggests that developing a representation of wind-forced snow redistribution in the model would significantly impact on the results and may be a lever for improving the simulated SDDs. We therefore recommend this kind of parameterization for snow density and thermal conductivity in sea ice models designed for climate studies.

[43] The mean snow depths on Arctic MYI (Figure 5) also indicate that runs with the smallest (largest) mean snow thermal conductivities produce the smallest (largest) snow depths. The reason is that a smaller snow thermal conductivity induces less heat carried into the inner snow-sea ice pack, therefore leading to an earlier onset of surface melt at the end of spring and a more intense thinning all along the snow melt period, and conversely. This also explains the early ice extent minimum of KLOW, which is shifted from September to August.

[44] Similar observations can be made in the SH, although for different reasons since surface melt conditions

Figure 8. Spatially integrated terms from the simulated mean sea ice mass balance (over 1979–2007), for (a) KPACK Arctic, (b) KLOW Arctic, (c) KPACK Antarctic, and (d) KLOW Antarctic. Positive (negative) diagnostics represent sea ice mass source (sink) terms. Snow ice formation corresponds to the surface production of sea ice whenever seawater floods the snow-sea ice interface and refreezes. Lateral production depicts the mass of sea ice forming in leads. Bottom production/melt and surface melt are the integrated diagnostics for the basal thermodynamic accretion/ablation of sea ice and the surface melt due to positive imbalance in the surface energy budget, respectively. There is no explicit lateral melting in the model.

are rarely reached there. As sea ice is thinner in KLOW (due to the limited bottom growth during winter), more snow ice production occurs due to more frequent negative freeboards and seawater flooding the snow-ice interface. This process, virtually nonexistent in the NH (see Figure 8, top), enhances the snow thinning but counterbalances the sea ice thermodynamic thinning. The latter mechanism partly explains why, in the SH, the differences in ice thickness between all runs are still small (as suggested by Table 2) relatively to the differences in mean snow thermal conductivity through the various formulations that are used. Furthermore, even though KLOW exhibits the smallest absolute deviations with regard to sea ice extent observations, it is the simulation with the smallest mean sea ice thickness and volume (not shown). The reason is that with

a smaller volume and minimum sea ice extent (see Figure 3), the larger area fraction of leads in late summer enables a more intense lateral growth of sea ice all along the following winter (Figure 8), hence compensating for the initial underestimation in the seasonal sea ice extent. Finally, the significantly less pronounced sensitivity of the SH sea ice thickness to the snow thermal conductivity representation is consistent with the findings of *Massonnet et al.* [2011]. They showed in particular that the NEMO-LIM3 SH ice concentration, extent, and thickness are less sensitive to the model physics compared to their NH counterparts, in the ORCA1 configuration. This result is due to the crucial importance of the oceanic heat supply in the Antarctic sea ice mass balance. Because the average value of this flux is larger in the SH, sea ice responds more

significantly to oceanic anomalies than to atmospheric ones, as already mentioned by *Maykut and Untersteiner* [1971].

6.2. Variability

[45] As shown by the model statistics, KLOW provides the smallest errors for the monthly sea ice extent anomalies with respect to observations in both hemispheres. However, only the 2 m air temperature and 10 m u-v winds bear an interannual component in our setup, while the other forcings (humidity, cloudiness, and precipitation) are climatological. Therefore, the full potential impacts of interannual variability and trends of the actual atmospheric state on the sea ice cover are only partially accounted for in our simulations. As an example, a significant trend in the Southern Ocean's precipitation in the context of a warming climate, as in *Zhang* [2007], would likely affect the sea ice extent anomalies and trends over the simulation period. Additionally, the restoring of the sea surface salinities toward the *Levitus* [1998] climatology further strengthens this problem. This in turn suggests limitations in the conclusions that can be drawn from our analysis of statistics in Table 2.

[46] KLOW simulation yields a smaller sea ice volume and a MYI areal coverage accordingly smaller, resulting in two consequences. First, the ice has a lower mass and responds faster to the dynamic forcing from the ocean and the atmosphere. Second, larger direct inputs of solar radiation are allowed into the ocean during the summertime drop in FYI concentration, affecting the heat budget in leads and the oceanic turbulent heat flux at the ice base. A positive ice-ocean feedback is then triggered as the bottom melt of the remaining ice is enhanced, subserving further decreases in ice concentration. Being aware of the aforementioned issues, the seemingly better ice extent variability in KLOW may therefore be attributed to larger oceanic interactions occurring during the simulation, while the impacts of the climatological forcing (clearly lacking of atmospheric feedbacks) are lessened. Nonetheless, this is to the detriment of the modeled sea ice mean volume, which seems to be remarkably underestimated, especially in the NH.

7. Conclusions

[47] A new snow thermodynamic scheme was embedded into the sea ice model LIM3 and the sensitivity of the global coupled ice-ocean model NEMO-LIM3 to the representation of snow thermal conductivity was assessed through four runs (at a $1°$ horizontal resolution) using different snow thermal conductivity formulations. These include a constant thermal conductivity (simulation KCST), relationships of *Yen* [1981] (KHIGH), *Sturm et al.* [1997] (KLOW), and a new one, based on *Domine et al.* [2011b] (KPACK), which is specifically designed for climate studies. The first result of this study is that the 0.31 W m^{-1} K^{-1} value for snow thermal conductivity, which is commonly used in large-scale sea ice models with a single-layer representation of snow, cannot be used in a multilayer snow scheme with varying density. This value, which seems too large, except for very dense snow, leads to an overestimation of the Arctic sea ice thickness, particularly in a multilayer scheme that is naturally more sensitive to the thermodynamic surface forcing than a single layer with constant thermophysical properties. None of these simulations provides good results in terms of all snow and ice variables and in both hemispheres simultaneously, which stresses the specific response of each hemisphere to varying snow physics. In the Arctic, the KPACK and KHIGH simulations give a reasonable estimate of the mean sea ice extent (absolute error between model and observations of 0.35×10^6 km^2 for KPACK, i.e. 2.8%) and thickness (absolute error of 0.63 m, KPACK) although the observed monthly sea ice extent anomalies over 1979–2007 are better reproduced with KLOW. In the Southern Ocean, KLOW leads to the minimum absolute errors, with mean values of 0.72×10^6 km^2 (10.5%) and 0.34 m ($\sim$30%) for ice extent and thickness, respectively. However, these better statistics may be due to compensating errors. Like in the NH, the sea ice basal thermodynamic growth is clearly curtailed by the low snow thermal conductivity values in the simulation, but it is partly compensated by both lateral production and snow ice formation maintaining the hydrostatic equilibrium of the snow-ice column. In the Arctic, low snowfall and thicker ice virtually prevent snow ice formation. KLOW also seems to feature a better sea ice variability compared to all other simulations, potentially allowing the oceanic feedbacks to play a more prominent role in driving the geographical distributions and temporal evolution of the ice concentration through the oceanic heat flux at the ice base. The new snow thermal conductivity formulation used in KPACK seems the only one reasonably well suited for both hemispheres even though the mean errors with respect to observed sea ice extent (1.01×10^6 km^2 (13.0%)) and thickness (0.37 m) are still quite large in the Southern Ocean, which could admittedly be due to other sources of errors in the simulation. The most important peculiarity of KPACK is its ability to reproduce the observed shape of the Snow Depth Distributions, thanks to relationships simply translating the effects the snow packing by wind, and indirectly influencing the snow depth. The importance of the Snow Depth Distributions in the model physics ultimately suggests that accounting for snow redistribution by the wind would presumably impact positively on the model performance. Finally, because of the lack of atmospheric feedbacks and the intrinsic limitations of the forcing, due to potential biases in the reanalyses and climatologies, those findings will have to be investigated using fully coupled configurations of the model, once available. This contribution stresses the need for further understanding of snow processes on sea ice and of efforts toward better representation in large-scale models.

References

Abels, G. (1892), Measurement of the snow density at Ekaterinburg during the winter of 1890–1891, *Acad. Nauk, Memoirs*, *69*, 1–24.

Berliand, M., and T. Strokina (1980), *Global Distribution of the Total Amount of Clouds*, 71 pp., Hydrometeorol., Leningrad.

Bitz, C., and W. Lipscomb (1999), An energy-conserving thermodynamic model of sea ice, *J. Geophys. Res.*, *104*(C7), 15,669–15,677.

Bouillon, S., M. Morales Maqueda, V. Legat, and T. Fichefet (2009), An elastic–viscous–plastic sea ice model formulated on Arakawa b and c grids, *Ocean Modell.*, *27*(3), 174–184.

Briegleb, B., and B. Light (2007), A Delta-Eddington multiple scattering parameterization for solar radiation in the sea ice component of the community climate system model, NCAR technical note, Tech. Rep. Note NCAR/TN-472+ STR, Natl. Cent. for Atmos. Res., Boulder, Colo.

Bromwich, D., et al. (2007), A tropospheric assessment of the ERA-40, NCEP, and JRA-25 global reanalyses in the polar regions, *J. Geophys. Res.*, *112*, D10111, doi:10.1029/2006JD007859.

Brun, E., E. Martin, V. Simon, C. Gendre, and C. Coleou (1989), An energy and mass model of snow cover suitable for operational avalanche forecasting, *J. Glaciol.*, *35*(121), 333–342.

Brun, E., I. Martin, and I. Spiridonov (1997), Coupling a multi-layered snow model with a GCM, *Ann. Glaciol.*, *25*, 66–72.

Calonne, N., F. Flin, S. Morin, B. Lesaffre, S. du Roscoat, C. Geindreau, F. St Martin dHeres, F. Grenoble, and I. Grenoble (2011), Numerical and experimental investigations of the effective thermal conductivity of snow, *Geophys. Res. Lett.*, *38*, L23501, doi:10.1029/2011GL049234.

Dai, A., and K. Trenberth (2002), Estimates of freshwater discharge from continents: Latitudinal and seasonal variations, *J. Hydrometeorol.*, *3*(6), 660–687.

Domine, F., J. Bock, S. Morin, and G. Giraud (2011a), Linking the effective thermal conductivity of snow to its shear strength and density, *J. Geophys. Res.*, *116*, F04027, doi:10.1029/2011JF002000.

Domine, F., L. Arnaud, J. Bock, C. Carmagnola, N. Champollion, J. Gallet, B. Lesaffre, S. Morin, and G. Picard (2011b), Vertical profiles of specific surface area, thermal conductivity and density of mid-latitude, arctic and Antarctic snow: Relationships between snow physics and climate, Abstract presented at 2011 Fall Meeting, AGU, San Francisco, Calif., 5–9 Dec. C32B-01.

Domine, F., J.-C. Gallet, J. Bock, and S. Morin (2012), Structure, specific surface area and thermal conductivity of the snowpack around barrow, Alaska, *J. Geophys. Res.*, *117*, D00R14, doi:10.1029/2011JD016647.

Dozier, J., and S. Warren (1982), Effect of viewing angle on the infrared brightness temperature of snow, *Water Resour. Res.*, *18*(5), 1424–1434.

Eicken, H., H. Fischer, and P. Lemke (1995), Effects of the snow cover on Antarctic sea ice and potential modulation of its response to climate change, *Ann. Glaciol.*, *21*, 369–376.

Fichefet, T., and M. Morales Maqueda (1997), Sensitivity of a global sea ice model to the treatment of ice thermodynamics and dynamics, *J. Geophys. Res.*, *102*(C6), 12,609–12,646.

Fichefet, T., B. Tartinville, and H. Goosse (2000), Sensitivity of the Antarctic sea ice to the thermal conductivity of snow, *Geophys. Res. Lett.*, *27*(3), 401–404.

Goosse, H. (1997), Modelling the large-scale behavior of the coupled ocean-sea ice system, PhD thesis, 231 pp., Univ. Catholique de Louvain, Louvain-la-Neuve, Belgium.

Goosse, H., and T. Fichefet (1999), Importance of ice-ocean interactions for the global ocean circulation: A model study, *J. Geophys. Res.*, *104*(C10), 23,337–23,355.

Grenfell, T., and G. Maykut (1977), The optical properties of ice and snow in the Arctic Basin, *J. Glaciol.*, *18*(80), 445–463.

Hellmer, H., M. Schröder, C. Haas, G. Dieckmann, and M. Spindler (2008), The Ispol drift experiment, ice Station POLarstern (ISPOL): Results of interdisciplinary studies on a drifting ice floe in the western Weddell Sea, *Deep Sea Res. Part II*, *55*(8-9), 913–917.

Holland, M., D. Bailey, B. Briegleb, B. Light, and E. Hunke (2012), Improved sea ice shortwave radiation physics in CCSM4: The impact of melt ponds and aerosols on Arctic sea ice, *J. Clim.*, *25*(5), 1413–1430.

Hunke, E., and J. Dukowicz (1997), An elastic-viscous-plastic model for sea ice dynamics, *J. Phys. Oceanogr.*, *27*(9), 1849–1867.

Järvinen, O., and M. Lepparanta (2011), Transmission of solar radiation through the snow cover on floating ice, *J. Glaciol.*, *57*(205), 861–870.

Kalnay, E., et al. (1996), The NCEP/NCAR 40-year reanalysis project, *Bull. Am. Meteorol. Soc.*, *77*, 437–471.

Kurtz, N., and S. Farrell (2011), Large-scale surveys of snow depth on Arctic sea ice from Operation IceBridge, *Geophys. Res. Lett.*, *38*, L20505, doi:10.1029/2011GL049216.

Kurtz, N., and T. Markus (2012), Satellite observations of Antarctic sea ice thickness and volume, *J. Geophys. Res.*, *117*, C08025, doi:10.1029/2012JC008141.

Kwok, R., B. Panzer, C. Leuschen, S. Pang, T. Markus, B. Holt, and S. Gogineni (2011), Airborne surveys of snow depth over arctic sea ice, *J. Geophys. Res.*, *116*, C11018, doi:10.1029/2011JC007371.

Langlois, A., C. Mundy, and D. Barber (2007), On the winter evolution of snow thermophysical properties over land-fast first-year sea ice, *Hydrol. Processes*, *21*(6), 705–716.

Large, W., and S. Yeager (2004), Diurnal to decadal global forcing for ocean and sea-ice models: The data sets and flux climatologies, National Center for Atmospheric Research (NCAR) Tech. Note TN-460+ STR. Boulder, Colorado, USA.

Lecomte, O., T. Fichefet, M. Vancoppenolle, and M. Nicolaus (2011), A new snow thermodynamic scheme for large-scale sea-ice models, *Ann. Glaciol.*, *52*(57), 337–346.

Ledley, T. (1985), Sensitivity of a thermodynamic sea ice model with leads to time step size, *J. Geophys. Res.*, *90*(D1), 2251–2260.

Levitus, S. (1998), NODC world ocean atlas. National Oceanographic Data Center (NODC-NOAA), Silver Spring, Maryland, USA [Available at http://www.esrl.noaa.gov/psd/.]

Madec, G. (2008), NEMO ocean engine. Institut Pierre-Simon Laplace (IPSL), Paris, France.

Massom, R., et al. (2001), Snow on Antarctic sea ice, *Rev. Geophys.*, *39*(3), 413–445.

Massonnet, F., T. Fichefet, H. Goosse, M. Vancoppenolle, P. Mathiot, and C. Beatty (2011), On the influence of model physics on simulations of Arctic and Antarctic sea ice, *Cryosphere*, *5*(3), 687–699.

Maykut, G., and N. Untersteiner (1971), Some results from a time-dependent thermodynamic model of sea ice, *J. Geophys. Res.*, *76*(6), 1550–1575.

Morin, S., F. Domine, L. Arnaud, and G. Picard (2010), In-situ monitoring of the time evolution of the effective thermal conductivity of snow, *Cold Reg. Sci. Technol.*, *64*(2), 73–80.

Nicolaus, M., C. Haas, J. Bareiss, and S. Willmes (2006), A model study of differences of snow thinning on Arctic and Antarctic first-year sea ice during spring and summer, *Ann. Glaciol.*, *44*(1), 147–153.

Nicolaus, M., C. Haas, and S. Willmes (2009), Evolution of first-year and second-year snow properties on sea ice in the Weddell Sea during spring-summer transition, *J. Geophys. Res.*, *114*, D17109, doi:10.1029/2008JD011227.

Perovich, D. (2007), Light reflection and transmission by a temperate snow cover, *J. Glaciol.*, *53*(181), 201–210.

Rothrock, D., D. Percival, and M. Wensnahan (2008), The decline in arctic sea-ice thickness: Separating the spatial, annual, and interannual variability in a quarter century of submarine data, *J. Geophys. Res.*, *113*, C05003, doi:10.1029/2007JC004252.

Semtner, A. (1976), A model for the thermodynamic growth of sea ice in numerical investigations of climate, *J. Phys. Oceanogr.*, *6*(3), 379–389.

Shine, K., and A. Henderson-Sellers (1985), The sensitivity of a thermodynamic sea ice model to changes in surface albedo parameterization, *J. Geophys. Res.*, *90*(D1), 2243–2250.

Sturm, M., and C. Benson (1997), Vapor transport, grain growth and depth-hoar development in the subarctic snow, *J. Glaciol.*, *43*(143), 42–59.

Sturm, M., and R. Massom (2009), Snow and sea ice, in *Sea Ice*, 2nd ed., edited by D. N. Thomas and G. Dieckmann, chap. 5, pp. 153–204, Wiley-Blackwell.

Sturm, M., J. Holmgren, M. König, and K. Morris (1997), The thermal conductivity of seasonal snow, *J. Glaciol.*, *43*(143), 26–41.

Sturm, M., K. Morris, and R. Massom (1998), The winter snow cover of the West Antarctic pack ice: Its spatial and temporal variability, in *Antarctic Sea Ice Physical Processes, Interactions and Variability*, edited by M.O. Jeffries, pp. 1–18, AGU, Washington, D. C.

Sturm, M., J. Holmgren, and D. Perovich (2002), Winter snow cover on the sea ice of the Arctic Ocean at the Surface Heat Budget of the Arctic Ocean (SHEBA): Temporal evolution and spatial variability, *J. Geophys. Res.*, *107*(C10), 8047, doi:10.1029/2000JC000400.

Taillandier, A., F. Domine, W. Simpson, M. Sturm, T. Douglas, and K. Severin (2006), Evolution of the snow area index of the subarctic snowpack in central Alaska over a whole season, consequences for the air to snow transfer of pollutants, *Environ. Sci. Technol.*, *40*(24), 7521–7527.

Tonboe, R., and E. Nielsen (2010), Global sea ice concentration reprocessing validation report, EUMETSAT Ocean and Sea Ice Satellite Application Facility (EUMETSAT OSISAF)., *Danish Meteorological Institute*, Product OSI-409, [Available at http://osisaf.met.no].

Trenberth, K., W. Large, and E. C. for Medium Range Weather Forecasts (1989), NCAR Trenberth wind stress climatology, Natl. Cent. for Atmos. Res., Boulder, Colo. [Available at http://dss.ucar.edu/datasets/ds110.1/].

Vancoppenolle, M., T. Fichefet, H. Goosse, S. Bouillon, G. Madec, and M. Maqueda (2009), Simulating the mass balance and salinity of Arctic and Antarctic sea ice, 1. Model description and validation, *Ocean Modell.*, *27*(1-2), 33–53.

Vancoppenolle, M., et al. (2011), Assessment of radiation forcing data sets for large-scale sea ice models in the southern ocean, *Deep Sea Res. Part II*, *58*(9), 1237–1249.

Vionnet, V., E. Brun, S. Morin, A. Boone, S. Faroux, P. Le Moigne, E. Martin, and J. Willemet (2012), The detailed snowpack scheme crocus and its implementation in SURFEX v7.2, *Geosci. Model Dev.*, *5*, 773–791.

Warren, S. (1982), Optical properties of snow, *Rev. Geophys. Space Phys.*, *20*(1), 67–89.

Worby, A., C. Geiger, M. Paget, M. Van Woert, S. Ackley, and T. DeLiberty (2008a), Thickness distribution of Antarctic sea ice, *J. Geophys. Res.*, *113*, C05S92, doi:10.1029/2007JC004254.

Worby, A., T. Markus, A. Steer, V. Lytle, and R. Massom (2008b), Evaluation of AMSR-E snow depth product over east Antarctic sea ice using in situ measurements and aerial photography, *J. Geophys. Res.*, *113*, C05S94, doi:10.1029/2007JC004181.

Wu, X., W. Budd, V. Lytle, and R. Massom (1999), The effect of snow on Antarctic sea ice simulations in a coupled atmosphere-sea ice model, *Clim. Dyn.*, *15*(2), 127–143.

Yen, Y. (1981), Review of thermal properties of snow, ice and sea ice, Rep. 81-10, U. S. Army Cold Reg. Res. and Eng. Lab. (CRREL), Hanover, N. H.

Zhang, J. (2007), Increasing Antarctic sea ice under warming atmospheric and oceanic conditions, *J. Clim.*, *20*(11), 2515–2529.

Corresponding author: O. Lecomte, Georges Lemaître Centre for Earth and Climate Research, Earth and Life Institute, Université catholique de Louvain, Louvain-la-Neuve, BE-1348, Belgium.